

# Numerical Analysis of Position Registration via Voltage Measurements

Bryan Nelson\* and Carl Toews†

## Abstract

This paper explores practical and numerical facets of a position registration scheme first proposed in [1]. The goal of the registration is to use voltage measurements to determine the shape of a bounded homogenous region embedded within an unknown and inhomogenous medium. We assume that a probe with one or more electrodes can access and be moved about within the region. At each of  $n$  discrete positions, each electrode records three voltages, one from each of three orthogonal fields that have been set up across the surrounding media. If the fields were linear, the position of the electrodes at each measurement could be read directly from the voltage data and the shape of the region inferred accordingly, but since the inhomogeneities in the surrounding media distort the fields, the problem becomes one of simultaneously calculating the electrode positions and the field distortions.

As in [1], here we model the field distortions as having a low-order expansion in some known functional basis, and attempt to solve for both the expansion coefficients and the probe positions via Gauss-Newton iteration. In this paper, our interest is focused on how well the reconstruction can be expected to succeed under variations in three factors: the choice of orientation parameters, the shape of the probe, and the expansion basis. Our results, which are supported which numerical experiments on simulated data, suggest that a proper attention to these factors can strongly influence the accuracy of the reconstruction.

## 1 Introduction

We consider the problem of locating the position and orientation of a rigid probe with multiple sensors located within a compact region  $\mathcal{B} \in \mathbb{R}^3$ . We assume that the probe can access and be moved within  $\mathcal{B}$  freely, but neither its position nor its orientation can be measured directly. Our goal is to use voltage readings to determine the position and orientation of the probe. Although  $\mathcal{B}$  will be assumed to be electrically homogenous, we will suppose that the region between  $\mathcal{B}$  and whatever apparatus is used to generate the voltage fields is of unknown and inhomogenous nature, as illustrated in Figure 1. The motivation for this problem comes from medical imaging, where  $\mathcal{B}$  might represent an interior organ and the distortions are induced by the surrounding body tissues.

One way to put this problem on mathematical footing is to suppose that there are three induced voltage fields, one in the  $x$ -direction, one in the  $y$  and one in the  $z$ . Without loss

---

\*Department of Mathematics, Duquesne University, Pittsburgh, PA 15282, email: nelson@duq.edu

†Department of Mathematics, Duquesne University, Pittsburgh PA 15282, email: toewsc@duq.edu

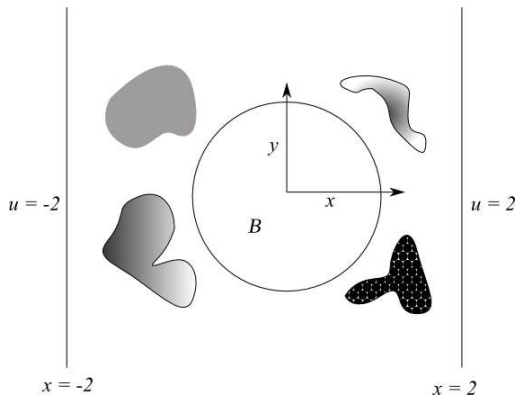


Figure 1: The probe can move freely within a bounded region, here illustrated by the circle. The textured lumps outside the circle represent the inhomogeneities that perturb the voltage fields.

of generality, we model these fields as

$$\begin{aligned}
 u(x, y, z) &= x + \pi_x(x, y, z), \\
 v(x, y, z) &= y + \pi_y(x, y, z), \\
 w(x, y, z) &= z + \pi_z(x, y, z),
 \end{aligned} \tag{1}$$

where  $\pi_x$ ,  $\pi_y$ , and  $\pi_z$  represent perturbations to the linear terms. If the probe is moved through  $n$  discrete positions, and at each position all  $m$  electrodes record each of the three voltage fields, then the (noise-free) data consists of  $3mn$  points given by

$$\begin{aligned}
 u_i^j &= x_i^j + \pi_x(x_i^j, y_i^j, z_i^j), \\
 v_i^j &= y_i^j + \pi_y(x_i^j, y_i^j, z_i^j), \\
 w_i^j &= z_i^j + \pi_z(x_i^j, y_i^j, z_i^j),
 \end{aligned} \quad i = 1 \cdots n; j = 1 \cdots m \tag{2}$$

where  $(x_i^j, y_i^j, z_i^j)$  denotes the euclidean coordinates of the  $j$ th electrode for the  $i$ th probe position. The goal is to use (2) to solve for the  $3mn$  unknowns  $(x_i^j, y_i^j, z_i^j)$ .

Without knowing the perturbation functions, this goal is clearly unachievable. However, if we assume that these functions have the form

$$\begin{aligned}
 \pi_x(x, y, z) &= \sum_{l=1}^{m_u} a_l \phi_l(x, y, z), \\
 \pi_y(x, y, z) &= \sum_{l=1}^{m_v} b_l \psi_l(x, y, z), \\
 \pi_z(x, y, z) &= \sum_{l=1}^{m_w} c_l \chi_l(x, y, z),
 \end{aligned} \tag{3}$$

for some known functional bases  $\{\phi_l\}$ ,  $\{\psi_l\}$ , and  $\{\chi_l\}$ , then we can use the data to solve for the expansion coefficients  $\{a_l\}$ ,  $\{b_l\}$ , and  $\{c_l\}$ . Although this approach would seem to

generate more unknowns than knowns, the number of unknowns can be reduced by recalling that since the probe is a rigid body, six parameters suffice to determine its general position (see [2].) Defining

$$\mathbf{s}_i := (x_i, y_i, z_i, \alpha_i, \beta_i, \gamma_i), \quad i = 1 \cdots n \quad (4)$$

to be the vector that specifies this position for the  $i$ th probe placement (where, e.g., the first three coordinates define the center of mass and the second three represent Euler angles) we can write

$$(x_i^j, y_i^j, z_i^j) = g^j(\mathbf{s}_i), \quad i = 1 \cdots n; j = 1 \cdots m, \quad (5)$$

where  $g^j$  is a known function that depends on the probe geometry. In particular,  $g^j$  can be written a translation and a rotation, i.e. as

$$g^j(\mathbf{s}_i) = (x_i, y_i, z_i) + R\mathbf{v}^j, \quad i = 1 \cdots n; j = 1 \cdots m, \quad (6)$$

where  $R$  is the rotation matrix specified by the Euler triple  $(\alpha_i, \beta_i, \gamma_i)$ , and  $\mathbf{v}^j$  is a vector defining the position of the  $j$ th electrode if the probe is centered at the origin and in some canonical position.

What emerges is thus an inverse problem in which the object is use the  $3mn$  data points (2) together with the perturbation model (3) and the sensor location equation (5) to solve for the  $6n$  position variables  $\mathbf{s}_i$  and the  $m_u + m_v + m_w$  expansion coefficients  $\{a_l\}$ ,  $\{b_l\}$ , and  $\{c_l\}$ . Note that as long as  $m > 2$  (i.e. the probe has at least three electrodes), the number of knowns will eventually exceed the number of unknowns and the problem will be formally well determined. The thrust of [1] was to show that a Gauss-Newton type solution to a slightly modified version of this problem was computationally promising.

This paper takes the Gauss-Newton approach as its starting point, and focuses on ways to improve the convergence of the Gauss-Newton iterates. It begins by addressing the impact of the choice of orientation parameters, weighing the conceptually simple Euler angles against the implementationally more complex but non-singular quaternions. It also explores the role of probe geometry, addressing the issue of whether or not a simple two-electrode probe of the sort studied in [1] can perform as well as a more complex, three-dimensional object. Lastly, it addresses the issue of basis functions, examining the issue of how choosing an orthogonal basis might minimize position reconstruction under modeling errors. Our results, which are a combination of analytic observation and numerical experiment, suggest that an attention to these details can make a significant difference in the quality of the estimation, and thus may be of use in guiding medical application of the idea.

The structure of this paper is as follows: the next section provides a quick review the Gauss-Newton approach and some of the algorithmic shortcuts developed in [1]. Section 3 is devoted to the issue of how best to represent probe orientation. It begins with a description of how to avoid constrained optimization when implementing the quaternions, and proceeds to a numerical examination of the practical impact of singular versus non-singular orientation coordinates. Section 4 deals with probe geometry. It focuses on two basic shapes, one a curved rod and the other a box, each with varying numbers of electrodes, and presents controlled numerical experiments to compare their relative efficiency. Section 5 discusses the impact of the choice of basis functions in the simplified setting of a one-dimensional problem. It considers two polynomial bases of the same degree, one orthogonal and one non-orthogonal, and examines the effect on position reconstruction under modeling errors in each. The last section contains a brief discussion of the significance of these results and a list of suggestions for future research.

## 2 The Gauss-Newton algorithm

This section provides a concise summary of the results in [1] relevant to what will follow. It is intended as a reference, and thus omits proofs and details. The reader interested in these matters should consult the original paper.

### 2.1 The algorithm

The Gauss-Newton method [3] can be brought to bear on this problem as follows: define a state vector  $\mathbf{S}$  as

$$\mathbf{S} = [\mathbf{s}^*; \mathbf{s}_1; \dots; \mathbf{s}_n],$$

where

$$\mathbf{s}^* := [a_1, \dots, a_{m_u}, b_1, \dots, b_{m_v}, c_1, \dots, c_{m_w}]^T \quad (7)$$

and the  $\mathbf{s}_i$  are as in (4). Define an observation vector  $\mathbf{O}$  as

$$\mathbf{O} := [u_1^1, v_1^1, w_1^1, \dots, u_n^m, v_n^m, w_n^m].$$

If  $\mathbf{F} : \mathbb{R}^{m_u+m_v+m_w+6n} \rightarrow \mathbb{R}^{3mn}$  is the forward map taking each  $\mathbf{S}$  to a unique  $\mathbf{O}$ , the least squares solution  $\hat{\mathbf{S}}$  is

$$\hat{\mathbf{S}} := \arg \min_{\mathbf{S}} \|\mathbf{F}(\mathbf{S}) - \mathbf{O}\|^2.$$

The Gauss-Newton algorithm finds  $\hat{\mathbf{S}}$  by solving a sequence of least square equations of the form

$$J(\mathbf{S}_k)^T J(\mathbf{S}_k) \delta \mathbf{S}_k = -J(\mathbf{S}_k)^T (\mathbf{F}(\mathbf{S}_k) - \mathbf{O}), \quad (8)$$

where  $\mathbf{S}_0$  is an initial guess,  $\mathbf{S}_k$  is the  $k$ -th update to that guess,  $J(\mathbf{S}_k)$  is the Jacobian of  $\mathbf{F}$  at  $\mathbf{S}_k$ , and  $\delta \mathbf{S}_k$  satisfies  $\mathbf{S}_{k+1} = \mathbf{S}_k + \delta \mathbf{S}_k$ .

### 2.2 The update step

Since the  $3m$  observations taken at a given probe placement have no bearing on the position parameters for any other placement, the observation vector can be decomposed into pieces

$$\mathbf{o}_i := (\mathbf{o}_i^1; \dots; \mathbf{o}_i^m), \quad \mathbf{o}_i^j = (u_i^j, v_i^j, w_i^j)^T, \quad (9)$$

whereupon the forward map can be written as stacked vectors  $\mathbf{f}(\mathbf{s}^*, \mathbf{s}_i)$ , where

$$\mathbf{f}(\mathbf{s}^*, \mathbf{s}_i) = \mathbf{o}_i, \quad i = 1 \dots n.$$

With this notation, the least squares estimate becomes

$$\hat{\mathbf{S}} := \arg \min_{\mathbf{S}} \sum_i \|\mathbf{f}(\mathbf{s}^*, \mathbf{s}_i) - \mathbf{o}_i\|^2.$$

As a consequence, the Jacobian  $J$  is sparse, with a general form

$$J = \left[ \begin{array}{c|ccc} U_1 & V_1 & 0 & \dots & \dots & 0 \\ U_2 & 0 & V_2 & 0 & \dots & 0 \\ \vdots & \vdots & & \ddots & & \vdots \\ \vdots & \vdots & & & \ddots & 0 \\ U_n & 0 & \dots & \dots & 0 & V_n \end{array} \right], \quad (10)$$

where  $U_i$  is the  $3m \times (m_u + m_v + m_w)$  matrix corresponding to  $\partial \mathbf{f} / \partial \mathbf{s}^*$  and  $V_i$  is the  $3m \times 6$  matrix corresponding to  $\partial \mathbf{f} / \partial \mathbf{s}_i$ . This sparsity engenders certain computational efficiencies. In particular, instead of solving the complete system (8) for the state update  $\delta \mathbf{S}_k$ , the update can be achieved piecewise by solving a succession of smaller systems. If we set

$$D := \sum_{i=1}^n U_i^T [1 - V_i(V_i^T V_i)^{-1} V_i^T] U_i, \quad (11)$$

then the update is given by  $\delta \mathbf{S}_k = [\delta \mathbf{s}^*, \delta \mathbf{s}_1, \dots, \delta \mathbf{s}_n]$ , where

$$\delta \mathbf{s}^* = D^{-1} \sum_{i=1}^n U_i^T [1 - V_i(V_i^T V_i)^{-1} V_i^T] [\mathbf{o}_i - f(\mathbf{s}^*, \mathbf{s}_i)], \quad (12)$$

and

$$\delta \mathbf{s}_i = (V_i^T V_i)^{-1} V_i^T [\mathbf{o}_i - f(\mathbf{s}^*, \mathbf{s}_i) - U_i \delta \mathbf{s}^*]. \quad (13)$$

In light of these simplifications, each iteration of the Gauss-Newton algorithm becomes:

1. For each  $i = 1, \dots, n$ , calculate the Jacobian sub-matrices  $U_i$  and  $V_i$ .
2. Use the  $U_i$  and the  $V_i$  to calculate  $D$  as in (11).
3. Invert  $D$  and use  $D^{-1}$  to calculate  $\delta \mathbf{s}^*$  as in (12).
4. For  $i = 1, \dots, n$  use  $\delta \mathbf{s}^*$  to calculate  $\delta \mathbf{s}_i$  using (13).
5. Update  $\mathbf{s}^* \leftarrow \mathbf{s}^* + \delta \mathbf{s}^*$ ; and  $\mathbf{s}_i \leftarrow \mathbf{s}_i + \delta \mathbf{s}_i$ , for  $i = 1, \dots, n$ .

Iterations will continue until some convergence criterion is reached.

### 3 Orientation Parameters

Equations (11)-(13) all involve inverting the quantity  $V_i^T V_i$ . Although the condition number of the full Jacobian depends on more than just the  $V_i$ , if the  $V_i$  are ill-conditioned the inversion algorithm using (11)-(13) will be as well. From the standpoint of experimental design, it thus makes sense to consider how particular parameter choices influence the condition numbers of these  $V_i$ , and, where possible, to choose parameters that make these matrices well-conditioned. This section formalizes and expands on this idea within the context of the choice of orientation parameters.

#### 3.1 Structure of the $V_i$

To streamline notation, we will write the state  $\mathbf{s}_i$  in (4) as

$$\mathbf{s}_i = (\mathbf{p}_i, \mathbf{q}_i),$$

where  $\mathbf{p}_i \in \mathbb{R}^3$  contains the center of mass coordinates and  $\mathbf{q}_i$  contains the orientation parameters. In equation (4)  $\mathbf{q}_i$  had dimension three, but as we wish to have a uniform treatment for both Euler angles and quaternions, here we refrain from specifying the size of  $\mathbf{q}_i$  and simply require that it contain some number of parameters that uniquely specify

a rotation matrix  $R$ . Irrespective of what these parameters might be, the map taking  $\mathbf{s}_i$  to the position  $\mathbf{e}_i^j$  of the  $j$ th electrode has the form of the map  $g^j$  defined in (6).

With this convention, we can decompose each  $V_i$  into two blocks as

$$V_i = [A_i | B_i] = \begin{bmatrix} A_i^1 & | & B_i^1 \\ \vdots & & \vdots \\ A_i^m & | & B_i^m \end{bmatrix} \quad (14)$$

where  $A_i$  is the total derivative of  $\mathbf{f}$  with respect to the center of mass, evaluated at  $\mathbf{p}_i$ ,  $B_i$  is the total derivative of  $\mathbf{f}$  with respect to the angle parameters, evaluated at  $\mathbf{q}_i$ , and the submatrices  $A_i^j \in \mathbb{R}^{3 \times 3}$  and  $B_i^j \in \mathbb{R}^{3 \times d}$  correspond to observations from the  $j$ th electrode. Letting  $\mathbf{e}_i^j$  denote the Euclidean coordinates of the  $j$ th electrode, we have the following formulas for  $A_i^j$  and  $B_i^j$ :

**Lemma 1.** *Each  $A_i^j$  is of the form*

$$A_i^j = \begin{bmatrix} u_x & u_y & u_z \\ v_x & v_y & v_z \\ w_x & w_y & w_z \end{bmatrix}, \quad (15)$$

where the subscripts denote partials and the partials are evaluated at  $\mathbf{e}_i^j$ . Each  $B_i^j$  is a matrix product of the form

$$B_i^j = A_i^j \cdot M^j, \quad M^j(:, k) = \begin{bmatrix} \partial g_1^j / \partial q_k \\ \partial g_2^j / \partial q_k \\ \partial g_3^j / \partial q_k \end{bmatrix}, \quad (16)$$

where the expression on the right gives the  $k$ th column of  $M^j$ ,  $g^j = (g_1^j, g_2^j, g_3^j)$  is the function (6),  $q_k$  is the  $k$ th position parameter, and all partials are again evaluated at the  $\mathbf{e}_i^j$ .

*Proof.* Let  $V_i^j$  denote the sub-matrix  $[A_i^j | B_i^j]$ . The data model (2) shows that the  $k$ th column of  $V_i^j$  is of the form

$$V_i^j(:, k) = \begin{bmatrix} \partial u / \partial s_k \\ \partial v / \partial s_k \\ \partial w / \partial s_k \end{bmatrix},$$

where  $s_k$  is the  $k$ th component of the state and each partial is evaluated at  $\mathbf{e}_i^j$ . Now  $u$ ,  $v$ , and  $w$  depend on the  $s_k$  through composition with the function  $g^j$  in (6), whence by the chain rule

$$\begin{bmatrix} \partial u / \partial s_k \\ \partial v / \partial s_k \\ \partial w / \partial s_k \end{bmatrix} = \begin{bmatrix} u_x & u_y & u_z \\ v_x & v_y & v_z \\ w_x & w_y & w_z \end{bmatrix} \cdot \begin{bmatrix} \partial g_1^j / \partial s_k \\ \partial g_2^j / \partial s_k \\ \partial g_3^j / \partial s_k \end{bmatrix}.$$

This gives (16), since the parameters for the  $B_i^j$  are simply the  $q_k$ . The simpler form of the  $A_i^j$ 's follows by writing out the components of  $g^j$  as

$$\begin{aligned} g_1^j &= x + P_{\hat{\mathbf{e}}_1} R \mathbf{v}^j \\ g_2^j &= y + P_{\hat{\mathbf{e}}_2} R \mathbf{v}^j \\ g_3^j &= z + P_{\hat{\mathbf{e}}_3} R \mathbf{v}^j, \end{aligned}$$

(where the  $P_{\mathbf{e}_k}$  represent projection onto the normalized standard basis vectors) and explicitly differentiating with respect to  $x$ ,  $y$ , and  $z$  to show that

$$\begin{bmatrix} \partial g_1^j / \partial x & \partial g_1^j / \partial y & \partial g_1^j / \partial z \\ \partial g_2^j / \partial x & \partial g_2^j / \partial y & \partial g_2^j / \partial z \\ \partial g_3^j / \partial x & \partial g_3^j / \partial y & \partial g_3^j / \partial z \end{bmatrix} = \begin{bmatrix} 1 & 0 & 0 \\ 0 & 1 & 0 \\ 0 & 0 & 1 \end{bmatrix}.$$

□

### 3.2 Quaternions

If the orientation parameters are Euler angles, then the  $M^j$  in Lemma 1 are square, whence so are the  $B_i^j$ 's. The  $V_i$  can either be calculated numerically, or, if the basis functions are sufficiently simple (e.g. polynomials), the above formulas can be used to calculate them analytically. In either case, after each Gauss-Newton iteration the angle vector  $\mathbf{q}_i$  is updated as part of the state update via the matrix multiplication (13).

If the orientation parameters are quaternions, then  $M^j \in \mathbb{R}^{3 \times 4}$ . In this case, the state vector  $\mathbf{s}_i$  is a 7-tuple of the form  $\mathbf{s}_i = (\mathbf{p}_i, \mathbf{q}_i)$ , where  $\mathbf{q}_i \in \mathbb{R}^4$  and  $\|\mathbf{q}_i\| = 1$ . Although the  $A_i$ 's and the  $B_i$ 's can be calculated just as with the Euler angles (i.e. numerically or analytically), the update step is complicated by the fact that each quaternion needs to lie on  $S^3$ , and this cannot be guaranteed using (13).

In order to avoid using constrained optimization, we use an idea developed in [4]. Recall that the exponential map  $\exp : \mathbf{R}^3 \rightarrow S^3$ , given by

$$\exp(\mathbf{w}) = (\cos \|\mathbf{w}\|, \sin \|\mathbf{w}\| \hat{\mathbf{w}}), \quad (17)$$

takes any element  $\mathbf{w} \in \mathbb{R}^3$  to a quaternion representing a rotation by  $\|\mathbf{w}\|$  radians around the unit vector  $\hat{\mathbf{w}}$ . In order to exhaustively explore all rotations in the neighborhood of a fixed quaternion  $\mathbf{q}$ , it thus suffices to consider all rotations of the form

$$\exp(\mathbf{w}) * \mathbf{q}, \quad (18)$$

where  $*$  represents quaternion multiplication and  $\mathbf{w} \in \mathbb{R}^3$  lies in a small neighborhood of the origin.

We can use this fact as follows: instead of working directly with the state  $\mathbf{s}_i \in \mathbb{R}^7$ , we define a new state  $\tilde{\mathbf{s}}_i := (\mathbf{p}_i, \mathbf{w}_i)$  and consider the modified forward map

$$\tilde{\mathbf{f}}(\mathbf{s}^*, \tilde{\mathbf{s}}_i) := \mathbf{f}(\mathbf{s}^*, \mathbf{p}_i, \exp(\mathbf{w}_i)\mathbf{q}_i). \quad (19)$$

To find the  $\tilde{\mathbf{s}}_i$  that minimize the sum of the errors  $\|\mathbf{o}_i - \tilde{\mathbf{f}}(\mathbf{s}^*, \tilde{\mathbf{s}}_i)\|^2$ , we seek perturbations  $\delta\tilde{\mathbf{s}}_i$  from initial guesses of  $\tilde{\mathbf{s}}_i = (\mathbf{p}_i, 0, 0, 0)$ . The least square solution for these perturbations can be found using the algorithm of Section 2, and the sub-states  $\mathbf{s}_i$  updated via  $\mathbf{p}_i \leftarrow \mathbf{p}_i + \delta\mathbf{p}_i$  and  $\mathbf{q}_i \leftarrow \exp(\delta\mathbf{w}_i) * \mathbf{q}_i$ .

Note that with this modified update scheme, the matrices  $M^j$  in Lemma 1 are once again square, since the partials are with respect to the  $\mathbf{w}_i$  instead of the  $\mathbf{q}_i$ . It turns out that these  $M^j$  have nice expressions in terms of cross-products. To streamline notation, define a matrix-vector cross-product between matrix  $M \in \mathbb{R}^{3 \times d}$  and vector  $\mathbf{v} \in \mathbb{R}^3$  as

$$M \times \mathbf{v} := [M(:, 1) \times \mathbf{v} \quad M(:, 2) \times \mathbf{v} \quad \cdots \quad M(:, d) \times \mathbf{v}], \quad (20)$$

where  $M(:, k)$  denotes the  $k$ th column of  $M$ . With this notation, we have the following compact expression for  $M^j$ :

**Lemma 2.** *In the setting of the Gauss-Newton scheme with forward map (19), the matrices  $M^j$  in equation (16) can be written*

$$M^j = R(I \times \mathbf{v}^j), \quad (21)$$

where  $R$  and  $\mathbf{v}^j$  are as in (6).

The formal proof is a straightforward but somewhat tedious exercise in vector calculus. The following sketch contains the main ideas.

*Sketch of proof.* Consider first the case where  $\mathbf{p}_i = (0, 0, 0)$  and  $\mathbf{q}_i$  is the identity quaternion. By (6), the columns of  $M$  will be given by

$$M(:, k) = \lim_{\|\delta \mathbf{w}_k\| \rightarrow 0} \frac{R(\exp(\delta \mathbf{w}_k)) \mathbf{v}^j - \mathbf{v}^j}{\|\delta \mathbf{w}_k\|},$$

where  $\delta \mathbf{w}_k$  is a small perturbation of the form  $(w, 0, 0)$ ,  $(0, w, 0)$ , or  $(0, 0, w)$  for  $k = 1, 2$ , and  $3$ , respectively, and  $R(\mathbf{q})$  denotes the rotation matrix induced by the quaternion  $\mathbf{q}$ . Since the matrices  $R(\exp(\delta \mathbf{w}_k))$  represent clockwise rotations of  $w$  radians around the  $x$ -,  $y$ -, and  $z$ -axes, it is an easy geometric exercise (using, e.g., the Law of Cosines) to see that the numerator of this expression can be written

$$R(\exp(\delta \mathbf{w}_k)) \mathbf{v}^j - \mathbf{v}^j = R(\exp(\delta \mathbf{w}_k/2)) \cdot (\hat{\mathbf{e}}_k \times \mathbf{v}^j) \cdot \sqrt{2 - 2 \cos(w)},$$

whereupon the result follows by the calculation

$$\begin{aligned} \lim_{\|\delta \mathbf{w}_k\| \rightarrow 0} \frac{R(\exp(\delta \mathbf{w}_k)) \mathbf{v}^j - \mathbf{v}^j}{\|\delta \mathbf{w}_k\|} &= \lim_{w \rightarrow 0} R_k(\exp(\delta \mathbf{w}_k/2)) \cdot (\hat{\mathbf{e}}_k \times \mathbf{v}^j) \cdot \frac{\sqrt{2 - 2 \cos(w)}}{w} \\ &= I \cdot (\hat{\mathbf{e}}_k \times \mathbf{v}^j) \cdot 1 \\ &= \hat{\mathbf{e}}_k \times \mathbf{v}^j. \end{aligned}$$

If  $\mathbf{p}_i$  is not the origin or  $\mathbf{q}_i$  not the identity, then the same argument can be applied to the vector  $p_i + R\mathbf{v}^j$  rotated around the transformed axes  $\mathbf{p}_i + R\hat{\mathbf{e}}_i$ . The proof follows identically, except the cross product  $\hat{\mathbf{e}}_k \times \mathbf{v}^j$  is replaced by the cross product

$$(\mathbf{p}_i + R\hat{\mathbf{e}}_i) \times (p_i + R\mathbf{v}^j) = R\hat{\mathbf{e}}_i \times R\mathbf{v}^j = R \cdot (\hat{\mathbf{e}}_k \times \mathbf{v}^j)$$

which yields the form given in the Lemma.  $\square$

### 3.3 Condition numbers

Lemma 1 shows that for any choice of orientation parameters the matrices  $B_i^j$  will have the form (16), and Lemma 2 shows that this form simplifies to (21) if the orientation parameters are taken to be the quaternions. Note that in all cases the formulas for the  $B_i^j$ 's depend on the  $\mathbf{v}^j$ 's, and these depend on an arbitrary choice of ‘‘canonical orientation’’, i.e. a choice of a body-fixed coordinate system with its origin at the center of mass. Since any two such body fixed coordinate systems  $\{\hat{\mathbf{r}}_k\}_{k=1}^3$  and  $\{\hat{\mathbf{s}}_k\}_{k=1}^3$  will be related by a unitary transformation  $U$  such that  $\hat{\mathbf{r}}_k = U\hat{\mathbf{s}}_k$ , the same holds true for the corresponding electrode position vectors  $\{\mathbf{v}_r^j\}$  and  $\{\mathbf{v}_s^j\}$ , i.e.

$$\mathbf{v}_r^j = U\mathbf{v}_s^j$$

The purpose of this section to show that in the case of the quaternions, this  $U$  has no effect on the condition of  $V_i$ , while for Euler angles the difference can be significant.

We begin with two simple lemmas that will be useful in what follows.

**Lemma 3.** *Consider a partitioned matrix of the form  $[A|B]$ , where  $A \in \mathbb{R}^{m \times p}$  and  $B \in \mathbb{R}^{m \times q}$ . If  $U \in \mathbb{R}^{q \times q}$  is unitary, then  $\text{cond}([A|B]) = \text{cond}([A|BU])$ .*

*Proof.* It is trivial to see that for any matrix  $M$  and any unitary matrix  $U$ ,

$$\text{cond}(M) = \text{cond}(MU).$$

The proof of the lemma follows by factoring the matrix  $[A|BU]$  as

$$[A|BU] = [A|B] \begin{pmatrix} I_p & 0_q \\ 0_p & U \end{pmatrix}, \quad (22)$$

and observing that if  $U$  is unitary, so is the matrix on the right hand side.  $\square$

In the following, let  $M \times \mathbf{v}$  denote the matrix-vector cross product defined in (20).

**Lemma 4.** *For any matrix  $M \in \mathbb{R}^{3 \times 3}$  and vector  $\mathbf{v} \in \mathbb{R}^3$ ,*

$$M \times \mathbf{v} = (I \times \mathbf{v})M.$$

*Proof.* The proof is a simple calculation:

$$\begin{aligned} M \times \mathbf{v} &= [M(:,1) \times \mathbf{v} \quad M(:,2) \times \mathbf{v} \quad M(:,3) \times \mathbf{v}] \\ &= \left[ \sum_1^3 m_{i1} \hat{\mathbf{e}}_i \times \mathbf{v} \quad \sum_1^3 m_{i2} \hat{\mathbf{e}}_i \times \mathbf{v} \quad \sum_1^3 m_{i3} \hat{\mathbf{e}}_i \times \mathbf{v} \right] \\ &= [\hat{\mathbf{e}}_1 \times \mathbf{v} \quad \hat{\mathbf{e}}_2 \times \mathbf{v} \quad \hat{\mathbf{e}}_3 \times \mathbf{v}] \cdot \begin{bmatrix} m_{11} & m_{12} & m_{13} \\ m_{21} & m_{22} & m_{23} \\ m_{31} & m_{32} & m_{33} \end{bmatrix} \\ &= (I \times \mathbf{v})M \end{aligned}$$

$\square$

We can now state and prove the main result regarding the quaternion-induced condition numbers of the  $V_i$ .

**Theorem 1.** *Let  $\{\hat{\mathbf{r}}_{\mathbf{k}}\}_{k=1}^3$  and  $\{\hat{\mathbf{s}}_{\mathbf{k}}\}_{k=1}^3$  be two different sets of probe-fixed coordinates with their origins at the center of mass. Let  $\mathbf{v}_{\mathbf{r}}^{\mathbf{j}}$  and  $\mathbf{v}_{\mathbf{s}}^{\mathbf{j}}$  denote the corresponding electrode position vectors, and  $V_r$  and  $V_s$  the respective quaternion-based Jacobian submatrices, calculated according to (15), (16), and (21). Then  $\text{cond}(V_r) = \text{cond}(V_s)$ .*

*Proof.* Partitioning  $V_r$  and  $V_s$  as

$$V_r = [A_r | B_r] \quad \text{and} \quad V_s = [A_s | B_s],$$

equation (15) shows that  $A_r = A_s$ . Letting  $A^j$  denote the common  $j$ th subblock of these matrices, we can use (21) to write

$$B_r^j = A^j R_r (I \times \mathbf{v}_{\mathbf{r}}^{\mathbf{j}}) \quad \text{and} \quad B_s^j = A^j R_s (I \times \mathbf{v}_{\mathbf{s}}^{\mathbf{j}})$$

for rotation matrices  $R_r$  and  $R_s$ . If  $U$  is the unitary matrix satisfying  $\hat{\mathbf{s}}_k = U\hat{\mathbf{r}}_k$  for all  $k$ , then it is easy to see that

$$\mathbf{v}_s^j = U\mathbf{v}_r^j \quad \text{and} \quad R_s = R_r U^T,$$

whence

$$\begin{aligned} B_s^j &= A^j R_s (I \times \mathbf{v}_s^j) \\ &= A^j R_r U^T (I \times U\mathbf{v}_r^j) \\ &= A^j R_r (U^T \times U^T U\mathbf{v}_r^j) \\ &= A^j R_r (I \times \mathbf{v}_r^j) U^T \\ &= B_r^j U^T, \end{aligned}$$

where the third equality follows from properties of the cross product and the fourth from Lemma 4. The result now follows by Lemma 3.  $\square$

While Theorem 1 does not imply that quaternions render the  $V_i$ 's well conditioned, it does subordinate the issue of condition to that of the physical positioning of the probe, rather than accidents of its body-fixed coordinate frame. Note that the same cannot be said of the Euler angles, since, for example, if the probe position is given by the Euler triple  $(\alpha, 0, \gamma)$ , perturbations in  $\alpha$  and  $\gamma$  correspond to the same motion, namely rotation around the  $z$ -axis. In these circumstances the matrix  $B_i$  will have two identical columns, whence  $V_i$  will have infinite condition number. If the middle variable is not exactly zero, but close, then a similar argument shows that the  $V_i$ 's will be non-singular but poorly conditioned. If, as in [1], we model the position and orientation of the probe as a random variable, and we suppose that orientation space is sampled uniformly, then the probability of generating one or more ill-conditioned  $V_i$  grows with the density of the sample, and goes to one as the number of samples goes to infinity. Since sampling as densely as possible is an important regularizing technique (see [1]), we conclude that the use of Euler angles induces an intrinsic tension in our efforts to stabilize the problem.

We record these observations as a corollary:

**Corollary 1.** *Using quaternions, the condition numbers of the  $V_i$  depend only on the perturbation fields, the probe geometry and the probe placement. Using Euler angles, the condition numbers of the  $V_i$  depend not just on these three factors but also the choice of a body-fixed coordinate frame. Moreover, for any such choice of Euler angles, certain  $V_i$  will be ill-conditioned with high probability as the number of samples goes to infinity.*

## 4 Probe Shape

Theorem 1 guarantees that if quaternions are used to represent orientation, the choice of body-fixed coordinates has no bearing on the condition of the  $V_i$ , but it does not say anything about what this condition might be. As noted earlier, the conditioning of these matrices depends on probe geometry, probe position, and the perturbation fields, but of these factors, only the geometry lies fully within the control of the researcher. The purpose of this section is to use the formulas developed in the last section to examine the behavior of the  $V_i$  under a range of probe shapes. It develops a general matrix decomposition model

that can be used to assess expected condition under a variety of probe configurations, and includes practical suggestions for how to adjust regularization parameters in response to this assessment.

#### 4.1 A one dimensional probe

We begin by considering the sensing device that formed the exclusive focus of [1], i.e. a simple two-electrode probe whose electrodes are separated by a distance  $2d$ . By symmetry, the two electrode position vectors  $\mathbf{v}^j$  in (6) satisfy  $\mathbf{v}^1 = -\mathbf{v}^2$ , whence by (14), (16) and (21), the  $V_i$  have the form

$$V_i = \begin{bmatrix} A_i^1 & A_i^1 R_i(I \times \mathbf{v}^1) \\ A_i^2 & -A_i^2 R_i(I \times \mathbf{v}^1) \end{bmatrix}. \quad (23)$$

**Lemma 5.** *The  $V_i$  induced by the two-electrode probe are singular.*

*Proof.* By Theorem 1, we can assume with no loss of generality that the  $\mathbf{v}^1$  in (23) is of the form  $(d, 0, 0)$ . Thus

$$I \times \mathbf{v}^1 = \begin{bmatrix} 0 & 0 & 0 \\ 0 & 0 & d \\ 0 & -d & 0 \end{bmatrix},$$

which in turn implies that  $V_i$  has a column of zeros.  $\square$

The singularity of the  $V_i$  corresponds to the fact that perturbations around the probe's axis of symmetry are unobservable. To accomodate this fact, the orientation of the two-dimensional probe should really be characterized not by six parameters but rather by five, as was done in [1]. One way to deal with the column of zeros is to eliminate it, keeping only the last two columns and reducing the size of  $V_i$  to  $3m \times 5$ . For coding purposes, however, it is computationally cumbersome to have to reshape the  $V_i$  whenever the probe exhibits an axis of rotational symmetry. An equivalent but more elegant solution is to achieve the same answer by strategically regularizing the inversion of the full matrix  $V_i^T V_i$ . If SVD truncation is the regularization method, such a strategy corresponds to choosing the singular value threshold to lie somewhere between 0 and the second smallest singular value of the  $V_i$ . Although in practice estimating the second smallest singular value may be difficult, it becomes easier as the distortions become smaller. This is the content of the following.

**Lemma 6.** *For the two-electrode probe, the second smallest singular value of the  $V_i$  goes to  $d$  in the limit as the distortions vanish.*

*Proof.* By (23), the matrix  $V_i^T V_i$  is given by

$$V_i^T V_i = \left[ \begin{array}{c|c} A_i^{1T} A_i^1 + A_i^{2T} A_i^2 & (A_1^{1T} A_1 - A_2^{2T} A_2)(I \times \mathbf{v}^1) \\ \hline (I \times \mathbf{v}^1)^T (A_1^T A_1 - A_2^T A_2) & (I \times \mathbf{v}^1)^T (A_i^{1T} A_i^1 + A_i^{2T} A_i^2)(I \times \mathbf{v}^1) \end{array} \right].$$

By the data model (2), the matrices  $A_i^j$  converge pointwise to the identity as the distortions vanish, whereupon  $V_i^T V_i$  converges pointwise to the matrix

$$V_i^T V_i := \left( \begin{array}{c|c|c} 2I_3 & 0 & 0 \\ \hline 0 & 2d^2 I_2 & 0 \\ \hline 0 & 0 & 0 \end{array} \right), \quad (24)$$

whose singular values are 1 and  $d^2$ . Since  $d \ll 1$  and the singular values of  $V_i^T V_i$  are the squares of the singular values of  $V_i$ , the result follows.  $\square$

Note that the proof really only requires that the each  $A_i^j$  be of the form  $A_i^j = cU$  for some scalar  $c$  and unitary matrix  $U$ , which will be the case whenever the fields  $u$ ,  $v$ , and  $w$  have orthogonal gradients of identical magnitude. Moreover, (24) reveals not just that the second largest eigenvalue of  $V_i$  is  $d$ , but that the largest eigenvalue is 1, from which it follows that the condition number of  $V_i$  is  $1/d$ . We record these observations as a corollary.

**Corollary 2.** *If throughout the region  $\mathcal{B}$  the fields  $u$ ,  $v$ , and  $w$  have orthogonal gradients of identical magnitude, then the two-electrode probe induces  $V_i$  whose condition number is  $1/d$ , where  $d$  is the distance between electrodes.*

In practice, of course, we expect neither the distortions to be negligible nor the fields to satisfy the conditions of Corollary 2. However, to the extent deviations from orthogonality can be quantified, these results could be used to provide at least order of magnitude calculations for the condition of the matrix inversions in the reconstruction algorithm. Even in the presence of large distortions, the gradients might be locally orthogonal (or nearly so), in which case the above results would represent reasonable approximations as long as the probe were small relative to the scale on which the gradients changed. While we feel this idea might profitably be exploited on the level of experimental design, its effectiveness will clearly be application-specific. We will return to this theme in the section on numerical results.

## 4.2 A two dimensional probe

Although the  $V_i$  induced by a two-electrode probe are necessarily singular, the  $V_i$  for a probe with unambiguous three-dimensional orientation may be quite well behaved. Since it also the case that such probe will contain more than two electrodes, and thus generates more observables than the two-electrode probe, it seems plausible that such a probe might exhibit superior performance.

In order to tackle this question, we begin by considering a small class of simple, medically viable probes consisting of equispaced electrodes aligned along a circular arc. For simplicity, we will assume an odd number of electrodes, and if we take the base position of such a probe to be lying flat in the  $x$ - $y$  plane, centered at the origin and symmetric around the  $z$ -axis, then the unrotated, untranslated coordinates of the  $j$ th electrode will be

$$\mathbf{e}_i^j = \left( \frac{1}{\kappa} \sin j\kappa d, \frac{1}{\kappa} (1 - \cos j\kappa d), 0 \right), \quad j = \pm \left\{ 0, 1, \dots, \frac{m-1}{2} \right\}, \quad (25)$$

where  $\kappa$  is the curvature of the probe and  $d$  is the distance between electrodes along the arc of the probe.

As in the last section, it is easy to use formula (16) to calculate the matrices  $B_i^j$  explicitly. The result is

$$B_i^j = \frac{1}{\kappa} \begin{pmatrix} 0 & 0 & 1 - \cos j\kappa d \\ 0 & 0 & -\sin j\kappa d \\ -1 + \cos j\kappa d & \sin j\kappa d & 0 \end{pmatrix}. \quad (26)$$

Once again, if the distortions are small, or the fields have orthogonal gradients of approximately equal magnitude, then the  $A_i^j$  are (multiples) of unitary matrices, whereupon a calculation using (25) and (26) shows that  $V_i^T V_i$  is given by

$$\begin{aligned} V_i^T V_i &= \left( \begin{array}{c|c} \sum A_i^{jT} A_i^j & \sum A_i^{jT} A_i^j B_i^j \\ \hline \sum B_i^{jT} A_i^{jT} A_i^j & \sum B_i^{jT} A_i^{jT} A_i^j B_i^j \end{array} \right) \\ &= \left( \begin{array}{c|c} mI & \sum B_i^j \\ \hline \sum B_i^{jT} & \sum B_i^{jT} B_i^j \end{array} \right) \\ &\cong \left( \begin{array}{c|c|c} C_1 & 0 & 0 \\ \hline 0 & C_2 & 0 \\ \hline 0 & 0 & C_3 \end{array} \right), \end{aligned}$$

where the congruence in the third line means equal up to an exchange of rows or columns (i.e. up to a unitary transformation) and the  $2 \times 2$  submatrices  $C_i$  are given by

$$\begin{aligned} C_1 &= \frac{1}{\kappa^2} \begin{pmatrix} \kappa^2 m & 0 \\ 0 & \sum_j \sin^2 j\kappa d \end{pmatrix} \\ C_2 &= \frac{1}{\kappa^2} \begin{pmatrix} \kappa^2 m & \kappa \sum_j (1 - \cos j\kappa d) \\ \kappa \sum_j (1 - \cos j\kappa d) & 2 \sum_j (1 - \cos j\kappa d) \end{pmatrix} \\ C_3 &= \frac{1}{\kappa^2} \begin{pmatrix} \kappa^2 m & -\kappa \sum_j (1 - \cos j\kappa d) \\ -\kappa \sum_j (1 - \cos j\kappa d) & \sum_j (1 - \cos j\kappa d)^2 \end{pmatrix} \end{aligned}$$

The eigenvalues of  $V_i^T V_i$  will be the eigenvalues of the blocks  $C_i$ , and a short calculation shows that there are four of these:

$$\begin{aligned} \lambda_1 &= m && \text{(from } C_1, C_2, \text{ and } C_3) \\ \lambda_2 &= \frac{1}{\kappa^2} \sum_j \sin^2 j\kappa d && \text{(from } C_1) \\ \lambda_3 &= \frac{1}{\kappa^2} \left( \sum_j 1 - \cos j\kappa d \right) \left( 1 + \frac{1}{m} \sum_j \cos j\kappa d \right) && \text{(from } C_2) \\ \lambda_4 &= \frac{1}{\kappa^2} \left( \sum_j \cos^2 j\kappa d - \frac{1}{m} \left( \sum_j \cos j\kappa d \right)^2 \right) && \text{(from } C_3). \end{aligned}$$

If  $d$  and  $m$  are fixed, these eigenvalues (and thus the condition of the  $V_i$ ) depend only on the curvature  $\kappa$ . As  $\kappa \rightarrow 0$ ,  $\lambda_4 \rightarrow 0$ , and as  $\kappa \rightarrow \infty$ ,  $\lambda_2$ ,  $\lambda_3$ , and  $\lambda_4$  all go to zero. In other words, if the curvature is chosen to be either too small or too large, the matrix  $V_i$  becomes ill-conditioned.

Figure 2 shows how the eigenvalues  $\lambda_1$ ,  $\lambda_2$ , and  $\lambda_3$  change as a function of probe curvature. The figure shows that the curvature for which the electrodes evenly fill out a circle keeps all the eigenvalues away from 0. The problem can also be attacked analytically: it is an enjoyable exercise in single variable calculus to show that for any curvature, the eigenvalues  $\lambda_2$  and  $\lambda_3$  decrease monotonically (for curvatures up to  $2\pi/(m-1)d$ ) and the  $\lambda_i$  satisfy the relations  $\lambda_3 > \lambda_2$  and  $\lambda_4 = \lambda_3 - \lambda_2$ . The curvature corresponding to evenly

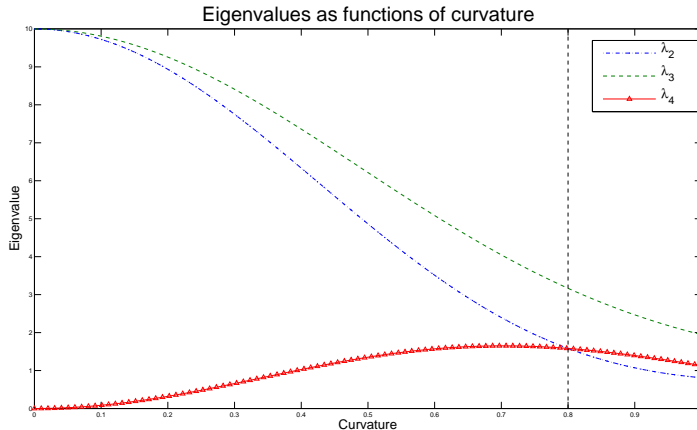


Figure 2: This plot shows the eigenvalues for the curved probe as a function of curvature. For this plot, the number of electrodes was 5, and the electrode separation distance was taken to be  $d = 1$ . Curvature is given as a fraction of the curvature  $\kappa_o := 2\pi/(m - 1)d$ , which is the curvature that brings the probe into a full circle, with the extremal electrodes overlapping. The black vertical line marks the curvature for which the electrodes evenly fill out a circle.

spaced electrodes is  $\kappa = 2\pi/md$ , and since at this curvature  $\lambda_4 = \lambda_2 = m^3d^2/8\pi^2$ , the corresponding condition number of the  $V_i$  becomes  $8\pi^2/m^2d^2$ . Although these calculations are tangential to the thrust of this paper, we record them for reference in the section on numerics:

**Lemma 7.** *If throughout the region  $\mathcal{B}$  the fields  $u$ ,  $v$ , and  $w$  have orthogonal gradients of identical magnitude, then the curved probe whose electrodes evenly fill out a circle induces a  $V_i$  whose condition number is  $8\pi^2/m^2d^2$ , where  $d$  is the distance between electrodes and  $m$  is the number of electrodes.*

As with our analysis of the two-electrode probe, we emphasize that in practice we do not expect the fields  $u$ ,  $v$ , and  $w$  to satisfy these orthogonality conditions strictly. On the other hand, we will see in the next section that this sort of analysis has predictive power in when the fields deviate considerably from this ideal. We also point out that this sort of analysis could be carried out for other probe shapes; we limit ourselves to these two, but clearly the range of probe shapes and size will be dictated by the physical constraints of the problem. These calculations should therefore be viewed as illustrative of the sort of information that might be considered when designing a probe, but by no means an algorithmic approach to such design.

## 5 Numerical Results

The last two sections have dwelt on the issue of how the conditioning of the matrices  $V_i$  can be expected to change under changes in both orientation parameters and the probe shapes. Although the condition of the full problem depends on more than just the  $V_i$ , we

have argued that since inversion of  $V_i^T V_i$  is an important and recurring operation in our version of the Gauss-Newton method, choosing parameters and equipment that optimize the condition of these matrices might be expected to positively impact the quality of the reconstruction. This section displays the results of several experiments that were designed to test this hypothesis.

We begin by considering the family of curved probes described in Section 4, i.e. probes with a fixed number of uniformly spaced electrodes arranged along the arc of a circle. We showed in the last section that as long as the fields  $u$ ,  $v$ , and  $w$  were orthogonal, the  $V_i$ 's were well conditioned whenever the electrodes evenly filled out the circle, and that the conditioned number was actually optimized if the circle had a slightly smaller curvature.

For our experiment, we took the region  $\mathcal{B}$  to be the cube  $[-1, 1]^3$ , and supposed that the distortions (2) were induced by degree two and three polynomials in three variables. Since there are 16 such polynomials, the coefficients  $\{a_i\}$ ,  $\{b_i\}$ , and  $\{c_i\}$  represent 48 unknowns. For our simulation, we generated these unknowns as Gaussian random variables with standard deviation 0.2, and then used these coefficient to generate the simulated observations corresponding to 480 random probe placements. Finally, we perturbed these observation with 1% Gaussian noise, and then tried to reconstruct both the coefficients and the electrode positions. We repeated this experiment for a range of curved probes, starting with one in which all the electrodes lay in a straight line and gradually increasing the curvature until the electrodes on the end overlapped.

Figure 3 gives an executive overview of the position reconstructions as a function of probe curvature. The  $x$ -axis gives curvature as a fraction of the critical curvature  $\kappa_0$ , defined as the curvature for which the terminal electrodes overlap. The  $y$ -axis gives the average position error, where the average is over both the electrodes and various realizations of the noise. The plot shows that the curvature which yields the best average reconstructions is between 0.6 and 0.7 of  $\kappa_0$ , which corresponds very closely to the value in Fig 2 which maximizes the condition number in a perturbation-free setting.

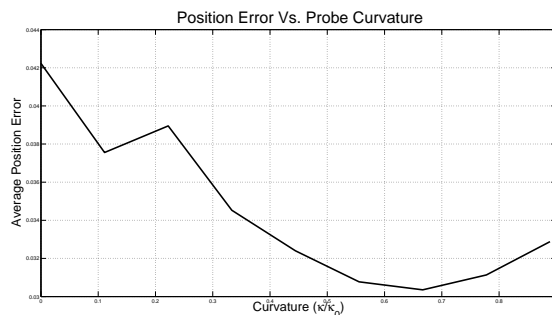


Figure 3: To generate this plot, we fixed one set of perturbation coefficients and allowed our probe to change curvature. For each value of the curvature, we perturbed the pseudo-observations under 10 realizations of the noise, reconstructing the positions via the Gauss-Newton algorithm for each such realization. The data represents position errors averaged first over the sample points and then over the various realizations of the noise.

We next turned our attention to a wider class of probes. In particular, we compared the performance of the two-electrode probe of [1], a curved probe, and a hypothetical “box”

probe with six electrodes located at distances  $\pm d$  along the  $x$ -,  $y$ -, and  $z$ -axes. We repeated the experiment as above, this time running a very large number of trials to generate reliable statistics.

Figure 4 give a picture of both the biases and variances of the coefficient reconstructions for all 48 coefficients and all three probes. The vertical bars stretch from the lowest reconstructed value to the larged reconstructed value, each according to the probe shape. The small horizontal bars show the true coefficient values. The figure clearly shows that the curved and box probes strongly out perform the 2-electrode probe, both in accuracy and precision.

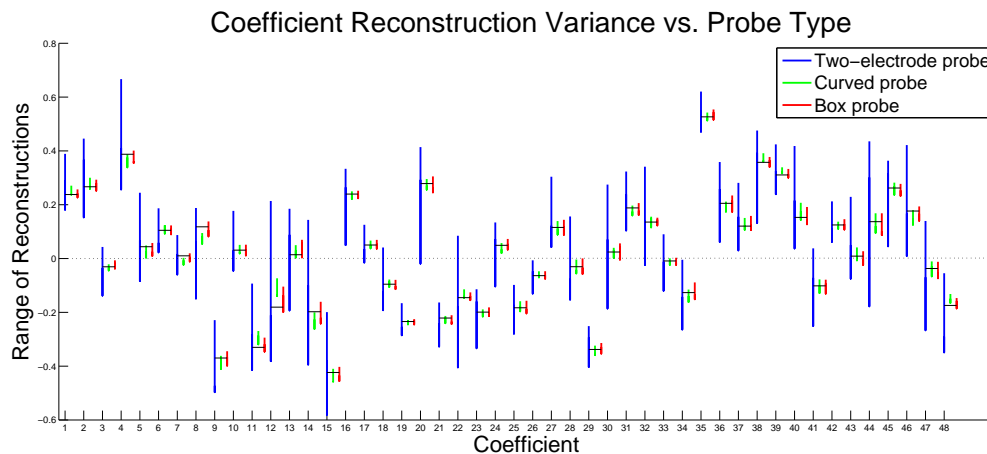


Figure 4: This plot shows how the variance of the coefficient reconstruction depends on the probe shape. To generate the plot, we generate one random set of 48 coefficients, corresponding to three complete sets of degree two and degree three polynomials in three variables. For each of three probes, we then reconstructed these coefficients under 125 instantiations of the noise. The vertical lines show the total range of the reconstructed values for each coefficient. The lines are grouped in set of three: the first corresponds to the two-electrode probe, the second to a curved probe, the third to a box-type model described in the text. Note that the results with the two-electrode probe are much less precise than with the other two.

Table 1 quantifies this performance in terms of the mean and variance of the reconstruction errors, defined variously as

$$\mathbf{s}_{\text{err}}^* := \frac{\|\hat{\mathbf{s}}^* - \mathbf{s}^*\|}{\|\mathbf{s}^*\|}$$

and

$$\mathbf{p}_{\text{err}}^* := \frac{\sum \|\hat{\mathbf{e}}_i^j - \mathbf{e}_i^j\|}{N},$$

where the carot denotes the estimate and the sum in the second equation is over all  $N$  electrode positions. Note that while the box probe outperforms the curved probe for error means, it performs slightly worse in terms of error variance. Both the box and the curved probe do significantly better than the two-electrode probe.

probe type	$\mathbf{s}_{\text{err}}^*$		$\mathbf{p}_{\text{err}}$	
	mean	std	mean	std
two-electrode	0.2581	0.0809	0.0795	0.0326
curved arc	0.0920	0.0088	0.0325	0.0025
box model	0.0587	0.0103	0.0198	0.0029

Table 1: *This table was generated from the same test run that generated Figure 3. The statistics show that the curved and box model probes yield better and more consistent estimates for both the coefficients and the positions.*

Our last experiment was designed to test the hypothesis that the quaternions work better than Euler angles. In this setting we limit ourselves to the two probes that yield full three-dimensional information, i.e. the curved probe and the box probe. For both of these probes the matrices  $V_i$  will typically not be singular, although their condition will vary from sample to sample. Our goal was see if these variations impacted the reconstructions.

For our experiment, we used the same set of 48 coefficients that were used to generate Table 1, and for each probe we tried to reconstruct them under variations in the sample pattern and noise values. For each sample/noise pair (i.e. for each set of observations), we ran the reconstructions twice, once with Euler angles and once with quaternions, and recorded which one produced the best reconstruction. We then calculated the P-values of these statistics, i.e. the probability of observing that many or more instances of quaternion superiority if in fact quaternions and Euler angles functioned equally effectively. The low P-values suggest that the superior numerical performance of the quaternions is not a fluke, but rather a fundamental feature of the problem.

probe type	Coefficients			Positions		
	Quat Wins	Eul Wins	P-value	Quat Wins	Eul Wins	P-value
curved arc	19	6	0.0073	17	8	0.0539
box model	18	7	0.0216	17	8	0.0539

Table 2: *We attempted to reconstruct the same 48 coefficients that were used to generate Table 1 under five different sample patterns and five different instantiations of the noise. We experimented with both the curved probe and the box probe, and we ran each reconstruction twice, once with quaternions and once with Euler angles. The columns Quat Mean and Eul Mean contain the solution errors for the quaternions and the Euler angles, respectively, averaged over all 25 trials. The P-Value column contains the probability that the observed number of trials in which the quaternions outperformed the Euler angles would be observed by chance if in fact the quaternions and the Euler angles were equally effective.*

Although Table 2 provide evidence that quaternions perform better than Euler angles, it is worth pointing out that the margin by which they achieve this superiority is not particularly large. With the curved probe, the quaternions improved the coefficient error by an average of 3.4% and the position error by an average of 0.8%, while with the box probe these improvements become 13.9% and 4.3%, respectively. Whether this level of improvement would persevere in a clinical setting and what the practical implications might

be are questions whose answers doubtless depend on particular applications.

## 6 Discussion

This paper has dwelt on the general problem of how to register the position of an electrode from readings of non-linear voltage fields. While the problem is motivated by specific medical applications, here we have attacked it in considerable generality, focusing on how probe shape and parameter choices influence the position estimates. The contributions of this paper include a theorem on conditioning invariance for certain Jacobian submatrices, concrete illustrations of how this theorem can be used to predict probe performance, and numerical results supporting the accuracy of these predictions.

The paper has left a number of crucial topics untouched. First among these is the issue of basis choice: while our numerical experiments used polynomials for ease of coding, there are many other choices, and it remains to be studied which can be used most profitably in which applications. There is also the issue of how best to regularize the problem, both on the level of the individual matrix inversions in our Gauss-Newton algorithm, but also in terms of how apriori information about the shape of the distortions can be brought to bear on the solution approach. In practice, the distortions may be quite large, and such apriori information could be of significant value. Lastly, it would be useful to generate some means of generating explicit estimates for the error terms, perhaps couched in terms of region geometry, distortion magnitude, noise level, and probe shape

## References

- [1] F. Santosa and C. Toews, *Position Registrations with Voltage Measurements*, Inverse Problems, 2007.
- [2] Landau, *Mechanics*
- [3] , *Numerical Optimization*
- [4] , *Nonlinear Least Squares Optimisation of Unit Quaternion Functions for Pose Estimation from Corresponding Features*
- [5] euler angles
- [6] quaternions